Journal of Power Sources 222 (2013) 1–9

Contents lists available at SciVerse ScienceDirect

Journal of Power Sources

journal homepage: www.elsevier.com/locate/jpowsour

Catalytic preferential oxidation of carbon monoxide over platinum supported on lanthanum ferrite–ceria catalysts for cleaning of hydrogen

Priti V. Gosavi, Rajesh B. Biniwale*

National Environmental Engineering Research Institute, Council of Scientific and Industrial Research, Nagpur-440020, India

HIGHLIGHTS

- Chitosan complex method resulted in $LaFeO_3$ with pure phase, crystalline, open porous morphology and higher surface area.
- Higher CO conversion in the range of 99% and selectivity for CO conversion in the range of 93–96%.
- Minimization of CO concentration in hydrogen to the extent of 30 ppm by PROX–CO reaction.
- Synergistic effect observed for PROX–CO activity using $LaFeO_3$ and CeO_2 as support for Pt catalyst.

GRAPHICAL ABSTRACT

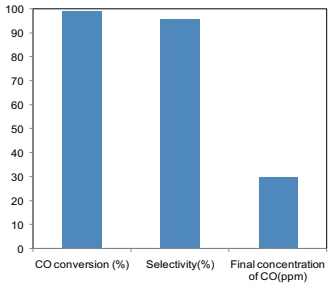

ARTICLE INFO

Article history:
Received 31 March 2012
Received in revised form
20 June 2012
Accepted 31 July 2012
Available online 31 August 2012

Keywords:
Preferential oxidation of carbon monoxide
Selective oxidation
Lanthanum ferrite catalysts
Effect of ceria and effect of platinum

ABSTRACT

Since hydrogen is produced by reforming of hydrocarbon it contains carbon monoxide (CO). In order to make hydrogen suitable for proton exchange membrane fuel cell application there is need to reduce concentration of CO less than 100 ppm. Water–Gas-Shift reactions subsequent to reforming lower CO concentration in H_2 to about 1–1.5% by volume. Preferential oxidation of CO (PROX–CO) using a catalyst is therefore important for further cleaning up of CO from H_2. The catalyst in this study is platinum supported over lanthanum ferrite–ceria ($Pt/LaFeO_3–CeO_2$) exhibits excellent activity of 99.8% and selectivity of 95.7% at a relatively lower temperature of 100 °C with an equivalence ratio of 3 for PROX–CO. The concentration of CO is reduced from 1% v/v in feed to ca. 30 ppm in product gas with relatively lower loss of hydrogen is the most significant achievement in this study. The catalyst is selective towards CO oxidation as the hydrogen loss is relatively low (ca. 3.8%) and there is no methane formation. The improvement in catalytic activity and selectivity is attributed to the strong metal support interaction and open morphology of catalyst. The results obtained in this study reveal the excellent catalytic activity by using $LaFeO_3–CeO_2$ as support for Pt catalyst.

1. Introduction

Availability of hydrogen free from contaminants such as CO and CO_2 is a prerequisite for fuel cell, particularly proton exchange membrane fuel cell (PEMFC) application. Hydrogen is produced from liquid hydrocarbons by the process of steam reforming or autothermal reforming. In addition to H_2, the product gas of reforming processes includes CO and CO_2. Presence of CO in hydrogen fuel above 100 ppm poisons the anode of PEMFC [1–3]. In order to reduce CO in reforming product gas, water–gas-shift (WGS) reactions are used. This reduces CO concentration to the extent of 1% v/v [4]. For further removal of CO from a hydrogen stream, catalytic preferential oxidation of CO (PROX–CO) remains one of the best choice [5]. Low cost, higher CO conversion and

* Corresponding author. Tel.: +91 712 2249885; fax: +91 712 224900.
E-mail addresses: gosavipriti@gmail.com (P.V. Gosavi), rb_biniwale@neeri.res.in (R.B. Biniwale).

0378-7753/$ – see front matter © 2012 Elsevier B.V. All rights reserved.
http://dx.doi.org/10.1016/j.jpowsour.2012.07.095

achieving desired low concentration of CO without excessive hydrogen consumption are some of the important attributes, which make PROX–CO method highly potential method for removal of CO from H_2 [6]. The PROX–CO catalysts must have higher selectivity towards oxidation of CO as compared to oxidation of H_2. Occurrence of WGS reaction on the catalysts surface at metal support has been reported as mechanism facilitating higher selectivity. The WGS reaction during PROX consumes CO converting H_2O back to H_2. Usually catalysts favour the reverse Water–Gas-Shift (r-WGS) reaction at a high temperature ($\Delta G_{rxn,298k} = +28.6$ kJ mol^{-1}). PROX–CO catalysts must inhibit the reverse water–gas-shift (r-WGS) reaction while should promote WGS reaction. Due to the exothermic nature of oxidation reactions and thermodynamics of WGS reaction, two adiabatic reactors are used in series in many commercial PROX–CO reactors [7–9]. The following reactions are carried out throughout the reaction.

$$CO + ½O_2 \rightarrow CO_2 \ (\Delta H_{rxn,298k} = -283 \text{ kJ mol}^{-1}) \quad (1)$$

$$H_2 + ½O_2 \rightarrow H_2O \ (\Delta H_{rxn,298k} = -242 \text{ kJ mol}^{-1}) \quad (2)$$

$$CO_2 + H_2 \rightleftarrows H_2O + CO\left(\Delta H_{rxn,298k} = +41.2 \text{ kJ mol}^{-1}\right) \quad (3)$$

Several metal catalysts such as Pt, Ru, Au, dispersed on metal oxides are promising catalysts for PROX–CO reaction. Similarly the transition metals such as Cu, CO and Fe are also used as catalysts for PROX–CO reaction [5,10,11]. The catalyst composition designs are targeted for promoting PROX–CO reaction mechanisms. There are several independent mechanisms proposed for PROX–CO namely non-competitive L–H mechanism, reaction of adsorbed CO and O_2 over bimetallic sites in closed vicinity and promotion of water–gas-shift reaction on Pt–CeO_2 interface subsequent to oxidation reaction. The PROX catalysts are reported to follow either of the reaction mechanisms.

Huang et al., reported Pt/Al_2O_3 and Ru/Al_2O_3 as catalysts to clean up CO in hydrogen. The feed composition for PROX reaction was 69% H_2, 28.5% CO_2, 0.5% CO and balance O_2. Increase in Pt and Ru content from 0.5 to 5 wt% in the catalysts reported to lower the temperature for complete CO conversion from 100 to 80 °C. However, methane formation was favoured using 5 wt% noble metal with an increase in temperature [10].

Tabakova et al. reported gold supported on Ce–Fe mixed oxides and compared the activity with Au/CeO_2 and Au/Fe_2O_3 catalysts. The feed used for PROX reaction was 1% CO, 1.25% O_2, 50% H_2 and balance He. Maximum CO conversion of 99.4% was observed for catalyst Au/CeO_2 at 110 °C. According to their report Fe_2O_3 addition to support helps to improve the resistance towards deactivation by CO_2 [11].

Similarly, Huang et al., suggested that addition of Fe to Pt/A_2O_3 and Ru/Al_2O_3 significantly enhanced the CO conversion rate below 160 °C. The CO conversion rate could be enhanced by adding cobalt for reactions carried out at temperatures above 200 °C [10].

According to the above discussions, it is evident that the roles of metal catalyst and support are important in PROX–CO reaction. Out of the various oxides, CeO_2 has been reported as one of the most preferred support for PROX–CO catalysts. CeO_2 fascinated the researchers due to high dispersion of active component over its surface and facilitation of PROX–CO mechanism through change in the oxidation state between 3+ and 4+, depending on redox conditions [12]. Use of mixed oxides is also reported as a potential alternative for PROX–CO reaction. CuO–CeO_2 exhibits higher CO conversion in presence of excess of hydrogen with lower oxygen excess (λ) [5]. Addition of Co_3O_4 in CeO_2 reported to impart stability to the catalyst. In addition to CO oxidation, mixed oxides CeO_2–Fe_2O_3 reported to exhibit catalytic activity for several reactions such as oxidation of p-cumaric acid, CO oxidation, CH_4 selective oxidation, Fischer–Tropsch synthesis and N_2O decomposition [13–17].

In spite of lower surface area of perovskite, their ability to involve lattice oxygen in reaction makes it as potential catalysts in various oxidation reactions. The studies reported for PROX–CO reaction over perovskite are limited. Some of the perovskite-based catalysts reported for PROX–CO include Pt/$Ce_xZr_{1-x}O_2$ [18] and CuO/$Ce_{1-x}Ti_xO_2$ [19]. $Ce_{0.8}Zr_{0.2}O_2$ and $Ce_{0.5}Zr_{0.5}O_2$ catalysts reported to exhibit CO conversion of 100% with selectivity of 50% at 65 and 91 °C respectively at $\lambda = 2$. For mixed oxides catalyst CuO/$Ce_{0.2}Ti_{0.8}O_2$, CO conversion of ca. 99.5% is reported at the temperature of 110 °C.

Perovskite $LaFeO_3$ is widely reported in the field of environmental catalysis [20]. PROX–CO is not reported over $LaFeO_3$. However the properties of Fe such as improving resistance towards deactivation by CO_2, desorption of oxygen etc. enhances CO oxidation at relatively lower temperatures. This study targets PROX–CO reaction over Pt/$LaFeO_3$ and to evaluate the effect of combination of $LaFeO_3$–CeO_2 as support for the reaction. The aim is to lower the CO concentration below 100 ppm with relatively lower hydrogen loss and without methane formation.

2. Experimental

2.1. Catalyst synthesis

The structure of chitosan–metal hydroxide complex is shown in Fig. 1. As reported for formation of alumina by chitosan complex route, NH_2 group of chitosan binds metal ions from salt solution [21]. During calcination chitosan is combusted and removed along with formation of metal oxides [22]. The removal of chitosan template during calcinations results into voids and help in formation of porous metal oxides. Similar approach could be followed for preparation of other metal oxides or mixed metal oxides. Therefore, we have synthesised perovskite $LaFeO_3$ by chitosan complex method. There may be a possibility of preferential uptake of a cation by chitosan and may result into the different chemical compositions of mixed metal oxide or perovskite. However, this can be controlled by carefully selecting cations and maintaining proper

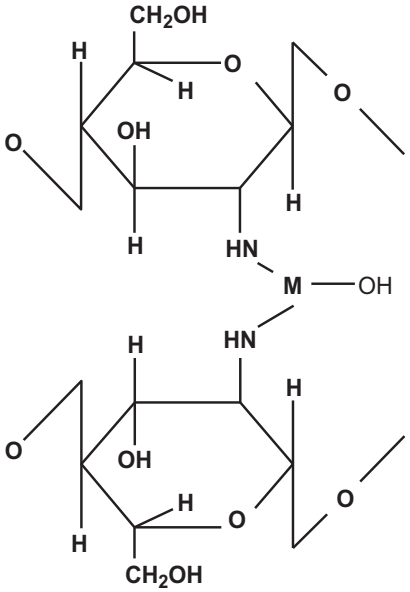

Fig. 1. Chitosan metal complex structure.

conditions during complex formation step such as to ensure proper mixing by stirring and to maintain mild temperatures.

The chitosan complex synthesis method has been already described in our previous publication [5]. However a brief description is given here. The ratio of metal ions, i.e. La and Fe with chitosan was 1:5 on a weight basis. A mixed aqueous solution of iron nitrate nonahydrate and lanthanum nitrate hexahydrate was added to the chitosan slurry (prepared by dissolving chitosan in 5% acetic acid). Subsequently, resultant slurry was precipitated in ammonia adding in a drop wise manner to form beads. The beads were then filtered and dried in an oven. Subsequently the dried mass was calcined upto 800 °C following a defined heating cycle.

In the synthesis of supported catalysts, CeO_2 (commercially available from eMerk, India) was added to the chitosan slurry before addition of nitrate solutions. Furthermore steps of synthesis are same as described above.

Pt loading was carried out by incipient wetting using a solution of chloro-platanic acid to obtain 0.5 wt% Pt/$LaFeO_3$–CeO_2, 1 wt% Pt/$LaFeO_3$–CeO_2, 2 wt% Pt/$LaFeO_3$–CeO_2 and 5 wt% Pt/$LaFeO_3$–CeO_2.

The $LaFeO_3$ synthesized using sol–gel method [23] was used to compare the activity, morphology and surface area with that of chitosan complex route. In order to differentiate $LaFeO_3$ synthesized using sol–gel method it was denoted as $LaFeO_3$ (SG). All other catalysts in this study have been synthesized using chitosan complex method.

2.2. Characterization of catalysts

Thermogravimetric analysis (TGA) of perovskite precursor was carried out using thermal analysor, Mettler Switzerland, Model-TA-4999, TG-50 with heating rate of 5 °C min^{-1}. XRD patterns of catalysts after complete calcinations were recorded on a Rigaku Miniflex II X-ray diffractometer, operated at 40 kV and 50 mA with a monochromator and using Cu-Kα radiation (λ = 0.15418 nm) within 2θ range of 20°–80°. Indexing of XRD peaks was carried out by using the JCPDS data for the respective phases. FTIR spectra were recorded on Bruker Vertex-70 by diffused reflectance accessory in the 4000–400 cm^{-1} range. The SEM investigations were carried out by JEOL JSM-6380-A instrument using 10.0 kV acceleration voltages. Surface area was measured by nitrogen adsorption using the automatic gas adsorption apparatus Micromeritics instrument model ASAP2010 and determined by BET method.

2.3. Catalytic reaction

A tubular glass reactor was used for carrying out catalytic test. About 100 mg of sample of catalysts were used for test. The catalysts were pre-treated using Ar with flow rate of 30 ml min^{-1} at temperature 500 °C for 2 h. The feed mixture used for catalytic test was having the composition of 50% hydrogen, 1% carbon monoxide, 1.5% oxygen on volume basis and balance by argon. Outlet gas was analyzed using Gas chromatograph (TCD detector) with separation column of molecular sieve 5A.

3. Results and discussion

3.1. Thermogravimetric analysis

Fig. 2 represents the TGA pattern obtained for precursor of $LaFeO_3$, where the synthesis route is chitosan complex route. The organic material which burns easily together with removal of residual nitrate, results in the sharp inflection point at 190 °C. The second inflection point between 320 and 380 °C indicates removal of residual carbon in the sample.

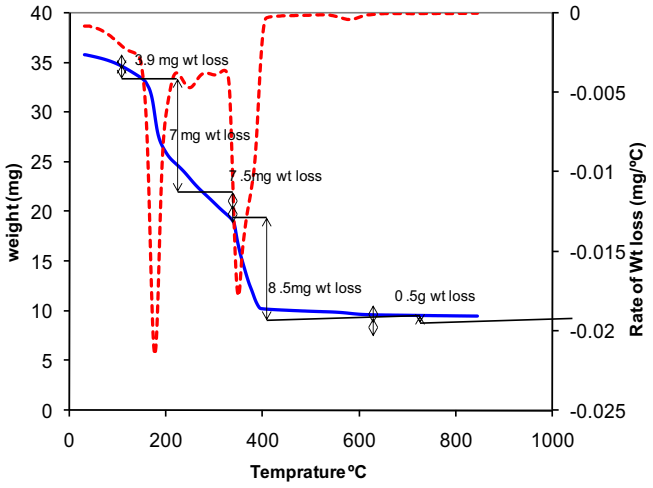

Fig. 2. TGA of precursor of $LaFeO_3$ synthesized using chitosan complex method.

The nature of TGA curve for precursor of chitosan complex route $LaFeO_3$ is as similar as in the case of Ni/Al_2O_3, using same method [22]. In a separate study, Fajardo et al. reports that, Ni doping promotes the removal of carbonaceous material at a lower temperature. Complete removal of residuals (carbon) from $LaFeO_3$ is observed at 400 °C which is analogous to study of Fajardo et al. Therefore the Fe is also expecting to behave as a promoter for elimination of carbonaceous residual by oxidation.

3.2. Catalyst phase formation

X-ray diffraction analysis confirms the phase formation of perovskites $LaFeO_3$. Fig. 3 represents the XRD patterns for $LaFeO_3$, $LaFeO_3$–CeO_2, 0.5 wt% Pt/$LaFeO_3$–CeO_2, 1 wt% Pt/$LaFeO_3$–CeO_2, 2 wt% Pt/$LaFeO_3$–CeO_2 and 5 wt% Pt/$LaFeO_3$–CeO_2, where the synthesis method is chitosan complex route. The XRD pattern in Fig. 3(a) is in good agreement with reported XRD data JCPDS 75-0541 for $LaFeO_3$. The XRD pattern indicates cubic crystal

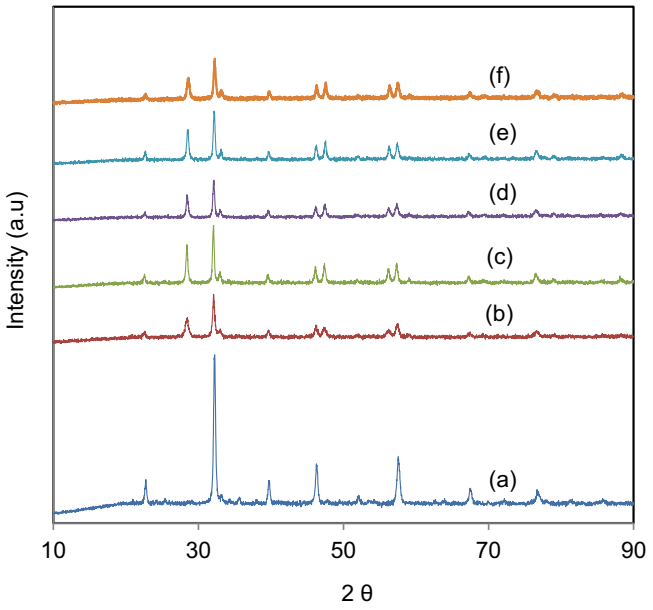

Fig. 3. XRD patterns of catalyst synthesized using chitosan complex route. (a) $LaFeO_3$, (b) $LaFeO_3$–CeO_2, (c) 0.5 wt% Pt/$LaFeO_3$–CeO_2, (d) 1 wt% Pt/$LaFeO_3$–CeO_2, (e) 2 wt% Pt/$LaFeO_3$–CeO_2 and (f) 5 wt% Pt/$LaFeO_3$–CeO_2.

structures for $LaFeO_3$ perovskite, with primitive lattice and lattice cell parameter a = 3.926 Å. When synthesis of perovskite is using chitosan complex route impurities of other phases are not observed in XRD pattern. This is an advantage of the chitosan complex method. Fig. 3(b) represents the XRD pattern of $LaFeO_3$–CeO_2, reveals both the phases of $LaFeO_3$ and CeO_2 which are confirmed with JCPDS card numbers 880641 and 810792 respectively. The $LaFeO_3$ phase present in the mixed oxide catalyst have primitive lattice, orthorhombic structure and lattice parameters a = 5.564 Å, b = 7.855 Å, c = 5.55 Å. The CeO_2 phase present in the catalyst have face centred cubic lattice, cubic structure and lattice parameter a = 5.4 Å. When $LaFeO_3$ is synthesized in presence of CeO_2 its structure is changed from cubic to orthorhombic. Such type of distortion in structure helps in enhancing the catalytic activity.

The XRD patterns of Pt-loaded $LaFeO_3$–CeO_2 are shown in Fig. 3(c)–(f) for Pt loading of 0.5 wt%, 1 wt%, 2 wt% and 5 wt% respectively. The peaks for Pt are not visible in Fig. 3 due to lower intensity however, a separate enlarged plot shown in Fig. 4 highlights the peaks for Pt at 2θ of 39.75° and 46.20°, present in the 5 wt % Pt/$LaFeO_3$–CeO_2 catalyst. The XRD patterns are in good agreement with JCPDS card no. 870646. The Pt present in the catalyst has face centred cubic structure and lattice parameter a = 3.920. The significant peaks for Pt were not seen in 0.5, 1, and 2 wt% Pt-loaded catalyst this may be attributed to lower quantity of Pt which cannot be detected by XRD.

Using Scherrer formula and full width of half maxima from XRD data, average crystalline size for $LaFeO_3$ in this study is estimated as 24.5 nm. Similarly, the average crystalline size of Pt loaded on different catalysts and CeO_2 are 29.18 nm and 48.64 nm respectively. The average crystalline size of $LaFeO_3$ is changed to 34.9 nm in presence of CeO_2.

3.3. FTIR analysis

Fourier Transformed infrared (FTIR) analysis spectra for $LaFeO_3$ (SG), $LaFeO_3$ synthesized using chitosan template method before calcination and $LaFeO_3$ synthesized using chitosan template method after calcination, are shown in Fig. 5(a)–(c) respectively. The FTIR analysis confirms the bonds present in perovskite phase.

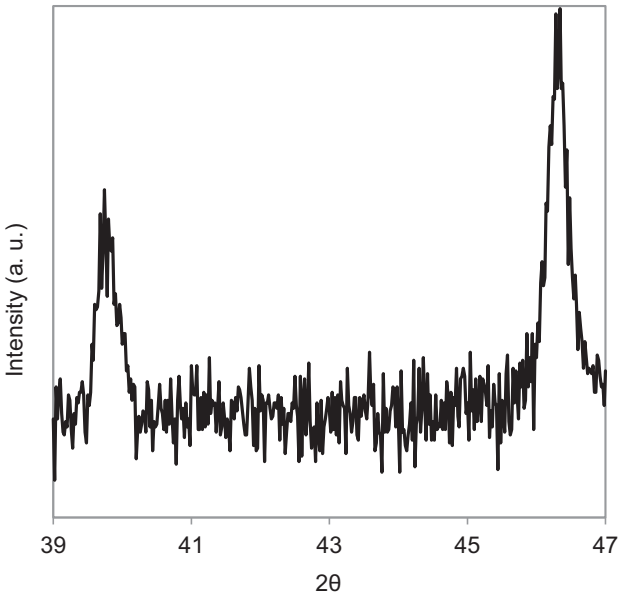

Fig. 4. XRD pattern depicting peak confirming the presence of Pt in 5 wt% Pt/$LaFeO_3$–CeO_2.

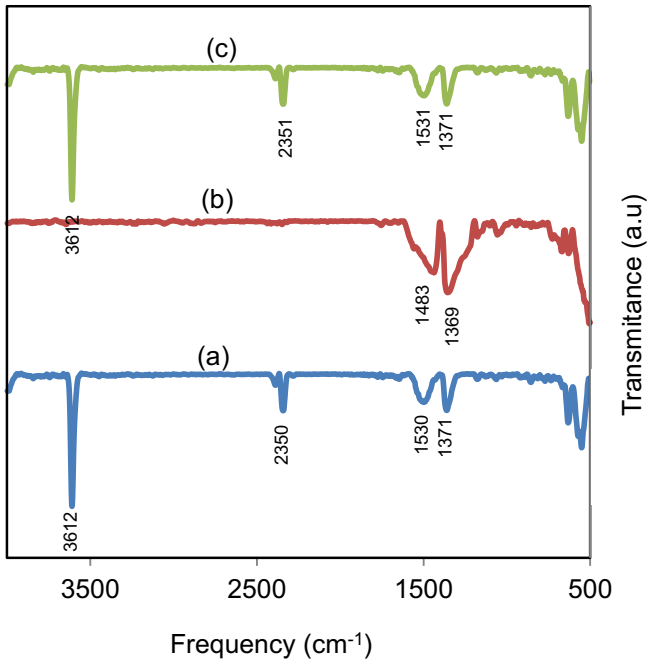

Fig. 5. FTIR spectra of (a) $LaFeO_3$ synthesized using sol–gel method, (b) $LaFeO_3$ synthesized using chitosan complex method (before calcination) (c) $LaFeO_3$ synthesized using chitosan complex method (after calcination).

Major FTIR peaks are in the range of wavenumber 3735–500 cm^{-1}. The FTIR patterns for $LaFeO_3$ (SG) and chitosan complex method are similar, which clearly implies similar phase formation. Since samples are exposed to atmosphere peaks observed at 3600 cm^{-1} and the range of 1380–1300 cm^{-1} are for O–H stretching [24] and adsorbed nitrogen oxide [25] respectively. The band appearing at 604 cm^{-1} is associated with oxide having perovskite-type structure [26]. In case of FTIR of precursor as shown in Fig. 5(b) peaks for La and Fe hydroxides generally occurring at 1600 cm^{-1} and 1800 cm^{-1} are not present. Therefore FTIR analysis confirms the formation of pure $LaFeO_3$ phase, which is also supported by XRD analysis.

3.4. Morphology of catalysts

Scanning Electron Micrographs (SEM) of perovskite $LaFeO_3$ (SG) and the chitosan template methods are depicted in Fig. 6(a) and (b). In a previous article we have reported formation of highly porous $LaFeO_3$ using sol–gel method [23]. The SEM of $LaFeO_3$ synthesized using chitosan complex method is compared with that of sol–gel method. It was evident that the chitosan complex route has produced highly porous and open structure than that of sol–gel route. Most of the pores are macro-pores. The open structure is particularly desirable for better access of reactant to active sites. This open structure may also be important for loading of a promoter (noble metal) when perovskite is used as a support for Pt.

Fig. 7(a) and (b) represents the SEM for $LaFeO_3$–CeO_2 and 5 wt% Pt/$LaFeO_3$–CeO_2 respectively. The SEM of $LaFeO_3$–CeO_2 at the magnification of 5000X and 10000X reveals the presence of different phases. The small particles present over the rigid phase may be of Fe, the rigid surface is considered of CeO_2. The improvement in catalytic activity may be due to this dispersed iron particle. The SEM for 5 wt% Pt/$LaFeO_3$–CeO_2 reveals dispersion of both Pt and Fe particles over CeO_2 and $LaFeO_3$. Furthermore, enhancement in catalytic activity may be attributes to dispersion of Pt. From the catalytic activity data for various catalysts of a synergistic effect is evident by using $LaFeO_3$–CeO_2 in combination as support for Pt.

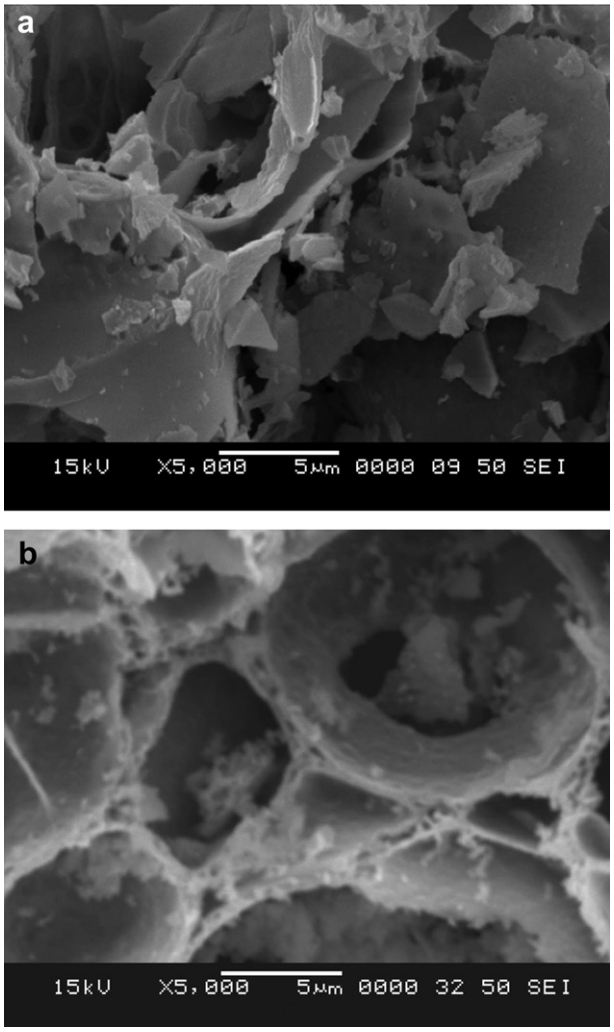

Fig. 6. SEM of $LaFeO_3$ synthesized using (a) sol–gel and (b) chitosan complex method.

3.5. Surface area

The surface area of perovskites is estimated by Brauner–Emmet–Taylor (BET) method of nitrogen adsorption. Improvement in the surface area from 16.5 to 22.95 $m^2\ g^{-1}$ for $LaFeO_3$ is obtained by using chitosan template method, when compared with $LaFeO_3$ (SG) catalyst.

3.6. Catalytic activity

3.6.1. CO conversion and effect of equivalence ratio on CO conversion

The PROX–CO reaction is carried out over $LaFeO_3$ (SG) and several catalysts synthesised by chitosan complex route. The catalysts prepared by chitosan route include $LaFeO_3$, $LaFeO_3$–CeO_2, 0.5 wt% Pt/$LaFeO_3$–CeO_2, 1 wt% Pt/$LaFeO_3$–CeO_2, 2 wt% Pt/$LaFeO_3$–CeO_2 and 5 wt% Pt/$LaFeO_3$–CeO_2. The catalysts can be ranked with respect to CO conversion as follows:

$LaFeO_3$ (SG) < $LaFeO_3$ < $LaFeO_3$–CeO_2 < 0.5 wt% Pt/$LaFeO_3$–CeO_2 ≈1 wt% Pt/$LaFeO_3$–CeO_2 ≈2 wt% Pt/$LaFeO_3$–CeO_2 ≈5 wt% Pt/$LaFeO_3$–CeO_2.

Results on activities of catalysts are shown in Fig. 8. The results on CO conversion and selectivity are listed in Table 1. The $LaFeO_3$ synthesized using sol–gel method exhibits in the CO conversion of 93.04% at 320 °C. CO conversion is improved to 95.25% in the case of $LaFeO_3$ synthesize using chitosan complex route at 320 °C. This improvement in activity is attributed to the relatively higher surface area. The use of CeO_2 as support for $LaFeO_3$ improves the CO conversion to 96.87% at a lower temperature of 250 °C. In order to estimate optimized loading of Pt 0.5–5 wt% is loaded on $LaFeO_3$–CeO_2 and evaluated for PROX–CO activity. Loading of 0.5 wt% Pt over $LaFeO_3$–CeO_2 exhibits 99.7% CO conversion at 250 °C. 1 wt% Pt loading over $LaFeO_3$–CeO_2 improves the CO conversion to 99.84% at lower temperature of 100 °C. Further increase in Pt loading does not improve the activity considerably. The improvement in CO conversion after increase in Pt loading is assigned to availability of more active site and promotion of WGS reaction at the interface of Pt–CeO_2 as reported in literature [27,28]. Similarly, Pt–$LaFeO_3$–CeO_2 provides not only the interface of Pt and CeO_2 but also provides the active surface and interface of Pt/$LaFeO_3$ for preferential oxidation and WGS reaction.

The excess mole ratio of oxygen is denoted by an equivalence ratio λ as a ratio of oxygen in feed to stoichiometric oxygen required for complete conversion of CO. Higher values of λ results into H_2 oxidation and is undesirable in PROX–CO reaction. Pozdnyakova et al., reported the dependency of PROX–CO activity on λ value. Accordingly, at $\lambda = 1$, CO conversion of 38% is achieved at 350 °C. At $\lambda = 2$, 100% CO conversion is achieved at 100–150 °C. However, at $\lambda = 4$, complete CO conversion is achieved at relatively higher temperature of 200 °C. In order to get higher selectivity, lower λ value of 2 is preferable [27]. When λ lies in between 1 and 2, 1 wt% Pt/CeO_2 exhibits the selectivity in the range of 99–100%. However, the CO conversion even at relatively higher temperature of 350 °C, is low i.e. 38% and 47% for $\lambda = 1$ and 2 respectively. Zepeda et al., report about 100% CO conversion on catalyst Au–hexagonal mesoporous silica–Fe at 150 °C and $\lambda = 4$ which obviously results in the lower selectivity ca 65% [29]. K–Rh/USY exhibits 99.5% CO conversion with 50% selectivity [30]. Tabakova et al. report Au/$Ce_{50}Fe_{50}$ (Ce–Fe mixed oxide support) catalyst, which exhibits 98.5% CO conversion at a lower temperature of 60 °C however, the selectivity is 42% [11]. Margitfalvi reports CO conversion at 60 °C over Au–$Fe_{0.4}$ of 83% [31]. Cu–CeO_2 converts 96% CO at 174 °C in both the case when λ is 2 and 4 [32]. One of our study reports 0.1 wt % Pt/$CuLaO_2$–CeO_2 catalyst, which exhibits 94.1% CO conversion with 87.2% selectivity at 320 °C and $\lambda = 0.3$ [5]. According to above discussion it's a trade off between temperature and λ for obtaining activity and selectivity. Increase in temperature or λ results into more oxidation of H_2 besides CO therefore with increase conversion, selectivity is lost. The catalyst in this study is designed to provide strong Pt-support interaction for promoting WGS reaction resulting into better activity and selectivity simultaneously. This study reveals the maximum 99.84% CO conversion with selectivity of 95.75% at 100 °C with $\lambda = 3$ over 1 wt% Pt/$LaFeO_3$–CeO_2 catalyst. Similarly, 0.5 wt% Pt/$LaFeO_3$–CeO_2 exhibits 99.74% CO conversion with 96.33% selectivity at 250 °C. The catalysts $LaFeO_3$ (SG), $LaFeO_3$, $LaFeO_3$–CeO_2, 2 wt% Pt/$LaFeO_3$–CeO_2 and 5 wt% Pt/$LaFeO_3$–CeO_2 also show the considerable higher CO conversion in the range of 93–99% and selectivity in the range of 71–96% between the temperature range of 100–320 °C.

3.6.2. H_2 conversion

The PROX–CO reaction is always associated with oxidation of hydrogen. The catalysts in this study are ranked with respect hydrogen loss as follows:

0.5 wt% Pt/$LaFeO_3$–CeO_2 < 1 wt% Pt/$LaFeO_3$–CeO_2 ≈2 wt% Pt/$LaFeO_3$–CeO_2 < 5wt% Pt/$LaFeO_3$–CeO_2 < $LaFeO_3$ < $LaFeO_3$–CeO_2 $LaFeO_3$ (SG).

The catalyst 0.5 wt% Pt/$LaFeO_3$–CeO_2 exhibits minimum hydrogen loss of 3.79%. The 1 wt% Pt/$LaFeO_3$–CeO_2 and 2 wt% Pt/$LaFeO_3$–CeO_2 exhibits hydrogen loss in the range of 4–4.5%.

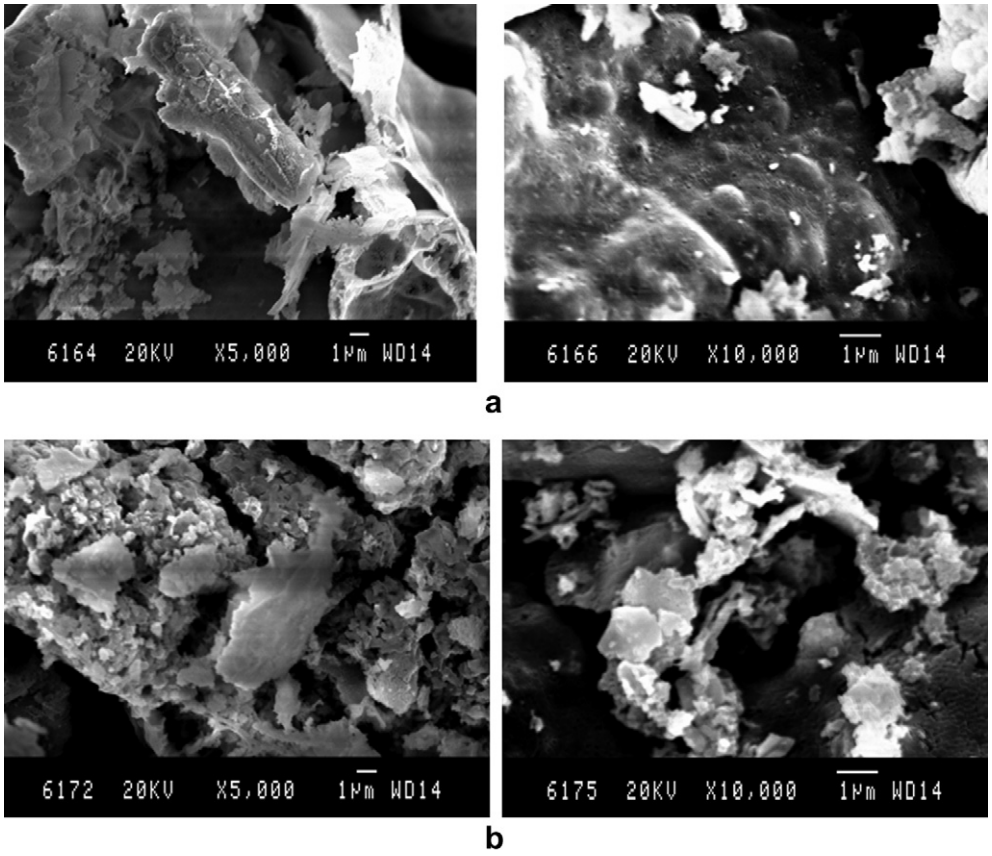

Fig. 7. SEM of (a) $LaFeO_3$–CeO_2 and (b) 5 wt% Pt/$LaFeO_3$–CeO_2 synthesized using chitosan complex route.

$LaFeO_3$ and $LaFeO_3$ (SG) exhibit 23.58% and 38.48% hydrogen loss respectively. The relatively lower hydrogen loss in case of 0.5 wt% Pt/$CuLaO_2$–CeO_2 catalyst may be due to promotion of WGS reaction on the surface resulting into higher selectivity of 95.7% towards CO conversion.

3.6.3. *CO/H_2 selectivity*

The catalysts in this study can be ranked with respect to CO/H_2 selectivity as follows:

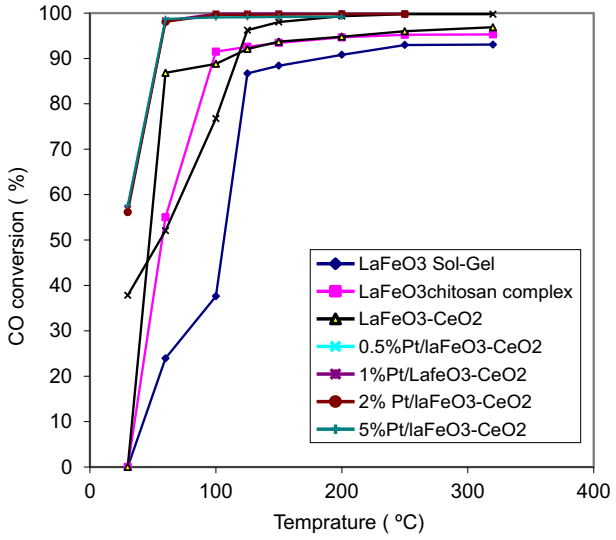

Fig. 8. Activity of catalysts for CO oxidation in presence of excess of hydrogen.

$LaFeO_3$ (SG) < $LaFeO_3$–CeO_2 < $LaFeO_3$ < 5 wt% Pt/$LaFeO_3$–CeO_2 < 1 wt% Pt/$LaFeO_3$–CeO_2 ≈2 wt% Pt/$LaFeO_3$–CeO_2 < 0.5 wt % Pt/$LaFeO_3$–CeO_2.

Pozdnakova et al., report the catalyst Pt/CeO_2 for PROX–CO and explain the reason for better activity [27]. Accordingly, Pt–CeO_2 interface promotes the WGS reaction. The WGS reaction recovers H_2 from H_2O, formed due to H_2 oxidation; to reduce net hydrogen conversion. As reported Pt sites have higher CO coverage. The CO adsorbed on Pt and oxygen adsorbed on support promotes the CO_2 formation. The oxygen present in feed re-oxidizes the CeO_2 surface. Hydrogen helps in maintaining higher concentration of cerium in Ce^{3+} form on the support surface which easily undergoes oxidation to convert into Ce^{4+} even at room temperature.

In the case of Pt/CeO_2, spill-over of oxygen from support to metal and vice-a-versa is possible. This facilitates the accumulation of carbonate species on support which at higher temperature undergoes decomposition and results into CO_2 and O_2. At lower temperature, Pt–ceria interface promotes the WGS reaction between linearly adsorbed CO molecule and water molecule. Oxygen deficiency in CeO_2 stabilizes the linearly bonded water molecules with Pt surface. Similar mechanism could be expected in the case of Pt-loaded $LaFeO_3$–CeO_2.

3.6.4. *Comparison of catalytic activities*

The activity, selectivity and resulting concentration of CO in product gas using various catalysts for PROX reaction are compared for various catalysts with this study in Table 1. The reported catalysts can be classified into various categories namely metal/metal oxide, bimetallic/metal oxide, mixed metal oxides, metals/zeolite etc. The attempts made in the previously reported articles are to achieve preferential oxidation of CO with relatively high selectivity

Table 1
Comparison of catalytic activity for CO–PROX reaction under various operating conditions.

Sr. no.	Catalysts	Oxygen excess (λ)	Temp (°C)	Initial concentration of CO (ppm)	Final concentration of CO (ppm)	CO conversion (mmol g^{-1} min^{-1})	CH_4 concentration (ppm)	H_2 consumed (%)	O_2 consumed	Selectivity for CO oxidation (%)	References
A: Noble metal/Metal oxide or mixed metal oxide											
1	1 wt% Pt/CeO_2	1	100	50,000	11,000	34.82	Nil	10	98	80	[35]
2	1 wt% Pt/ZrO_2	1	100	50,000	21,000	25.89	Nil	Not depicted	95	60	
3	1 wt% Pt/CeO_2	2	100	50,000	2500	42.4	Nil	~90	98	48	
4	1 wt% Pt/ZrO_2	2	100	50,000	1000	43.7	Nil	Not depicted	98	50	„
5	1 wt% Pt/CeO_2	1	350	10,000	6200	20.68	–	–	99	66	[27,28]
6	1 wt% Pt/CeO_2	2	110	10,000	1700	45.1	–	–	99	42	„
7	5 wt% Pt/CeO_2	1	350	10,000	5900	25.07	–	–	98	60	„„
8	5 wt% Pt/CeO_2	2	110	10,000	1600	51.36	–	–	99	43	„„
9	1 wt% Pt/Al_2O_3	–	100	5000	500	40.8	–	–	–	–	[10]
10	1 wt% Ru/Al_2O_3	–	140–160	5000	400	41.0	14,347	–	–	–	[10]
11	Au/$Ce_{50}Fe_{50}$ Ce–Fe mixed oxide support	2.5	70	10,000	150	87.94	–	–	–	42	[11]
12	0.32 wt% Pt/$Ce_{0.8}Zr_{0.2}O_2$	2	71	10,000	2920	44.0	–	–	–	50.1	[33]
13	2 wt% Pt/$Ce_{0.15}Zr_{0.85}O_2$	4	225	20,000	7000	31.6	–	–	~98	73	[36]
14	3 wt% Cu–CeO_2	1.5	147	20,000	1320	41.7	–	–	~99	66.4	[32]
15	3 wt% Cu–CeO_2	2	174	20,000	800	42.8	–	–	~99	49.9	„
16	3 wt% Cu–CeO_2	4	175	20,000	760	42.9	–	–	99	25.7	„
B: Metal oxide /metal oxide											
17	10 wt% CoO_x/CeO_2	2	175	10,000	0	44.64	275	22	99.9	–	[39]
C: Bimetal/Metal oxide											
18	K–Pt/A_2O_3	2	102–127	2000	10	44.64	–	–	–	–	[34]
19	0.5 wt% Fe–5 wt% Pt/Al_2O_3	2	80–170	10,000	2800	32.23	Could not be measured with available analytical equipments	–	100	67.3	[38]
20	0.1 wt% Pt/$CuLaO_2$–CeO_2	0.3	320	10,000	390	42.0	–	0.26	99.56	87.2	[5]
D: Metals or bimetals over zeolite											
21	K–Rh/USY	2	200	10,000	6000	44.41	–	–	99	38	[30]
22	4 wt% Pt–0.5 wt% Fe/Mordenite	2	200	10,000	2500	35.71	Nil	–	90	70	[37]
E: Noble metal/metal oxide–metal oxide											
23	Au–hexagonal mesoporous silica–CeO_2	4	60	5000	1250	11.16	35	–	81	76	[29]
F: $LaFeO_3$–CeO_2 supported catalysts											
24	$LaFeO_3$ (SG)	3	320	10,000	696	41.53	Nil	38.4	97.47	71.95	This study
25	$LaFeO_3$	3	320	10,000	470	42.5	Nil	23.58	89.86	80.16	
26	$LaFeO_3$–CeO_2	3	250	10,000	310	43.2	Nil	38.48	97.37	74.78	
27	0.5 wt% Pt/$LaFeO_3$–CeO_2	3	250	10,000	30	44.5	Nil	3.7	83.43	96.33	
28	1 wt% Pt/$LaFeO_3$–CeO_2	3	100	10,000	20	44.6	Nil	4.45	86.3	95.73	
29	2 wt% Pt/$LaFeO_3$–CeO_2	3	100	10,000	30	44.5	Nil	4.09	84.8	96.05	
30	5 wt% Pt/$LaFeO_3$–CeO_2	3	100	10,000	80	44.3	Nil	6.9	91.0	93.44	

towards CO and minimum loss of hydrogen. We compare the performance of other PROX catalysts and the catalysts in this study using following criteria:

- CO conversion activity both in terms of percentage conversion and mmol of CO converted per gram of catalyst per minute.
- Selectivity towards CO oxidation as compared to H_2 consumption or CH_4 formation.
- Initial concentration of CO used and final concentration of CO obtained in view of application to fuel cells.
- Excess of O_2 provided (in terms of equivalence ratio, λ).

Various mechanisms are proposed for preferential oxidation of CO. Pozdnyakova et al. [28], proposed a mechanism for PROX–CO over CeO_2 supported Pt catalysts. Accordingly, at a lower temperature, below 130 °C, the CO molecule is linearly adsorbed on Pt surface and H_2O molecule is adsorbed on CeO_2 surface. This facilitates the low temperature WGS reaction at Pt–CeO_2 interface. Such type of WGS reaction either may occur by direct reaction between CO and H_2O or may occur via carboxylate intermediate formation. At a higher temperature, the hydrogen bounded to Pt decomposes and water desorbs forming co-ordinatively unsaturated Ce^{n+} site at interface. In this situation CO can adsorb at the

interface in a bridge like manner with oxygen co-ordinating this unsaturated Ce^{n+} site. The adsorb CO then can react with OH group which results into formate. These formates are stable on CeO_2 which possibly avoid the adsorption of H_2O on the Pt. According to Kotobuki et al., [33] the pathway followed for PROX–CO reaction is Langmuir–Hinshelgwood mechanism for Pt/Mordenite catalyst. They have observed that O_2 and CO adsorb on Pt at lower temperatures. At temperatures above 120 °C, O_2 dissociates from the Pt surface and reacts with adsorbed CO. Therefore desorption of O_2 is a prerequisite. Pt–Fe/Mordenite follows the bi-functional mechanism with CO adsorbed on Pt and O_2 adsorption on Fe with subsequent reaction of adsorbed species. This facilitates reducing the temperature for the PROX–CO reaction to as low as 50 °C.

Role of OH group formed due to H_2 and O_2 adsorbed species is also discussed in the literature for promoting PROX–CO via auto-catalytic route involving OH. In this regards Kuriyama et al., reported the mechanism for potassium promoted PROX–CO reaction. Accordingly, potassium decreased the interaction between Pt and CO. This is due to increase in electron deficiency of the Pt. The OH groups formed due to adsorption of H_2 and O_2, are co-adsorbed with CO which facilitates the CO oxidation [34].

In the category of metal/metal oxide, the benchmark catalyst in the literature is Pt/CeO_2. There is a wide variation in Pt content of catalyst reported in the literature. However 1 wt% Pt/CeO_2 is an effective catalyst with proper dispersion of Pt. Wootsch et al., report catalytic activity over 1 wt% Pt/CeO_2 at temperature of 100 °C as 34.82 at $\lambda = 1$ and 42.4 mmol g^{-1} min^{-1} at $\lambda = 2$ where, the initial concentration CO is of 5% v/v. The final concentrations of CO reported are 1.1% and 0.25% respectively. With the increase in Pt content to 5 wt%, a relatively lower concentration of CO of 0.16% and relatively high catalytic activity of ca. 51 mmol g^{-1} min^{-1} is reached at temperature of 110 °C and λ of 2 over 5 wt% Pt/CeO_2. The comparison on the criteria of selectivity towards CO oxidation several catalysts 1 wt% Pt/ZrO_2, 5 wt%/CeO_2, 3 wt% Cu/CeO_2 exhibits relatively high selectivity in the range of 60–66%. However, 2 wt% $Pt/Ce_{0.15}Zr_{0.85}O_2$ and 1 wt% Pt/CeO_2 catalysts exhibit 31.6 and 34.8 mmol g^{-1} min^{-1} of catalytic activity for CO conversion and selectivity of 73 and 80% respectively. Accordingly, the role of CeO_2 is very evident with 1 wt% Pt/CeO_2 as one of the most potential catalyst. The reason for high selectivity is assigned in the literature to the mechanism of promotion of WGS reaction at Pt–CeO_2 interface [28,35,36].

Bimetallic catalysts such as K–Pt/Al_2O_3 resulted in 44.6 mmol g^{-1} min^{-1} of CO conversion activity with final concentration of CO as 10 ppm [34]. However the initial concentration of CO was 2000 ppm (0.2%) only. With relatively high initial concentration of CO of 1%, 4 wt% Pt–0.5 wt% Fe/Mordenite exhibits catalytic activity of 35.7 mmol g^{-1} min^{-1} with 70% selectivity towards CO conversion at temperature of 200 °C with λ of 2 [37]. Final concentration of CO achieved in this case is (2500 ppm) 0.25%. Similarly 0.1 wt% $Pt/CuLaO_2$–CeO_2 exhibits catalytic activity of 42 mmol g^{-1} min^{-1} with 87% selectivity at relatively higher temperature of 320 °C with oxygen deficient conditions [5]. The mechanism for bimetallic catalysts is via a reaction of adsorbed CO and O_2 over bimetallic sites in closed vicinity.

Relatively lower CO concentration in product gas is obtained with a high equivalence ratio. For example, at λ of 4, 3 wt% Cu/CeO_2 and Au/meso SiO_2 resulted in final concentration of 760 ppm and 1250 ppm starting from 20,000 ppm (2%) and 5000 ppm (0.5%) respectively [30,32]. Since metal Cu and support CeO_2 both promote oxidation reaction at relatively higher λ of 4 the selectivity is lower at ca. 25%. The same catalyst, 3 wt% Cu/CeO_2, exhibits catalytic activity of 42.8 mmol g^{-1} min^{-1}, selectivity of 49.9% and final concentration of CO of 800 ppm at $\lambda = 2$. Still further reduction in λ to 1.5 results in selectivity of 66% at a relatively lower temperature of 147 °C. However, the final concentration of CO was 1320 ppm. The non-competitive Langmuir–Hinshelgwood mechanism is mostly explained for these catalysts. Which implies reaction between CO adsorbed on Pt sites and oxygen activated on support [30,32].

A comparison of performances of catalysts in this study with the reported catalysts is shown in Table 1 [10,11,27,28,30,32–39]. Bare $LaFeO_3$ and $LaFeO_3$–CeO_2 converts CO in the range of 90–97% at temperatures in the range of 250–320 °C. The final concentration of CO is in the range of 310–700 ppm. With loading of 0.5 wt% Pt on $LaFeO_3$–CeO_2 catalytic activity of 44.5 mmol g^{-1} min^{-1}, selectivity of 96.3% and final concentration of CO of 30 ppm is obtained at the reaction temperature of 250 °C. The catalytic activity and selectivity is maintained while reaction temperature is decreased by increasing Pt content. When Pt content is 1 and 2 wt% over $LaFeO_3$–CeO_2 the hydrogen conversion is 4.45 and 4.09% with final concentration of CO as 20 and 30 ppm respectively. Herein, Pt–CeO_2 interface for promoting WGS reaction and non-competitive Langmuir–Hingshelwood mechanism is probably prevailing. Further, increase in Pt content to 5 wt% results in CO concentration of 80 ppm due to marginal increase in H_2 conversion to 6.9% and a slight decrease in CO conversion. Accordingly 1 wt% Pt/$LaFeO_3$–CeO_2, from this study exhibits excellent performance for PROX of CO.

4. Conclusions

The $LaFeO_3$ perovskite synthesized in this study using chitosan complex method is a material with several improved properties namely, phase purity, relatively higher crystalinity, better porosity with open structured morphology and higher surface area in comparison with sol–gel method. The Pt supported on mixed metal oxides catalysts exhibits relatively higher activity and selectivity concomitantly. Pt-loaded $LaFeO_3$–CeO_2 catalysts exhibited CO conversion and selectivity in the range of 99% and 93–96% respectively. The important conclusion of this study is that the product gas from PROX reaction is having CO concentration as low as 30 ppm with initial concentration of 1%. These results are most promising for cleaning of CO form H_2 generated via hydrocarbon reforming and render it suitable for fuel cell applications.

Acknowledgments

This work has been carried out under the Supra Institutional Project (SIP-16) of National Environmental engineering Research Institute, CSIR, Nagpur. A senior Research Fellowship awarded by CSIR to Priti Gosavi is gratefully acknowledged.

References

[1] M. Navarro, M.A. Pena, J.L.G. Fierro, Chem. Rev. 107 (2007) 3952–3991.
[2] A.J. Appleby, F.R. Foulkes, Fuel Cell Handbook, Van Nostrand Reinhold, New York, 1989.
[3] J.M. Zalc, D.G. Loffler, J. Power Sources 111 (2002) 58–64.
[4] F. Joensen, J.R. Rostrup-Nielsen, J. Power Sources 105 (2002) 195–201.
[5] P.V. Gosavi, R.B. Biniwale, Int. J. Hydrogen Energy 37 (2012) 3958–3963.
[6] E. Quinet, F. Morfin, F. Diehl, P. Avenier, V. Caps, J.L. Rousset, Appl. Catal. B: Environ. 80 (2008) 195–201.
[7] C.D. Dudefield, R. Chen, P.L. Adcock, Int. J. Hydrogen Energy 26 (2001) 763–775.
[8] H. Igarashi, H. Uchida, M. Suzuki, Y. Sasaki, M. Watanabe, Appl. Catal. A: Gen. 159 (1997) 159–169.
[9] C.D. Dudefield, R. Chen, P.L. Adcock, J. Power Sources 86 (2000) 214–222.
[10] C.-Y. Huyang, Y.-Y. Chen, C.-C. Su, C.-F. Hsu, J. Power Sources 174 (2007) 294–301.
[11] T. Tabakova, G. Avgouropoulos, J. Papavasilio, M. Manzoli, F. Boccuzzi, K. Tenchev, F. Vindigni, T. Ioannides, Appl. Catal. B: Environ. 101 (2011) 256–265.
[12] A. Troarelli, Catal. Rev. Sci. Eng. 38 (1996) 439–520.
[13] G. Neri, A. Pistone, C. Milone, S. Galvagno, Appl. Catal. B: Environ. 38 (2002) 321–329.
[14] H. Bao, X. Chen, J. Fang, Z. Jiang, W. Huang, Catal. Lett. 125 (2008) 160–167.

[15] K.Z. Li, H. Wang, Y.G. Wei, M.C. Liu, J. Rare Earths 26 (2008) 245–249.
[16] F.J. Perez-Alonso, M. Lopez Granadose, M. Ojeda, P. terrerose, S. Rosjas, T. Herranz, J.L.G. Fierro, M. Gracia, J.R. Gancedo, Chem. Mater. 17 (2005) 2329–2339.
[17] F.J. Perez-Alonso, I. Melian-Cabrera, M. Lopez Granadose, F. Kapteijs, J.L.G. Fierro, J. Catal. 239 (2006) 340–346.
[18] J.L. Ayastuy, M.P. Gonzalez-Marcos, A. Gil-Rodriguez, J.R. Gonzalez-Velasco, M.A. Gutierrez-Ortiz, Catal. Today 116 (2006) 391–399.
[19] Z. Wu, H. Zhu, Z. Quin, H. Wang, L. Huang, J. Wang, Appl. Catal. B: Environ. 98 (2010) 204–212.
[20] P. Ciambelli, S. Cmino, L. Lisi, M. Faticanti, G. Minelli, I. Pitteti, P. Porta, Appl. Catal. B: Environ. 33 (2001) 193–203.
[21] I.M.N. Vold, K.M.V. Arum, E. Guibal, O. Smidsr, Carbohydr. Polym. 54 (2003) 471–477.
[22] H.V. Fajardo, A.O. Martine, R.M. de Almeida, L.K. Noda, L.F.D. Probst, N.L.V. Carreno, A. Valentini, Mater. Lett. 59 (2005) 3963–3967.
[23] P.V. Gosavi, R.B. Biniwale, Mater. Chem. Phys. 119 (2010) 324–329.
[24] B. Vishwanathan, S. George, Ind. J. Technol. 23 (1985) 470–472.
[25] A.E. Ginnakas, A.K. Ladavos, P.J. Pomonis, Appl. Catal. B: Environ. 49 (2004) 147–158.
[26] S. Royer, F. Berube, S. Kaliaguine, Appl. Catal. A: Gen. 282 (2005) 273–284.
[27] O. Pozdnyakova, D. Teshner, A. Wootscha, J. Krohanert, B. Steinhauer, H. Sauer, L. Toth, F.C. Jentoft, A. Knop-Gericke, Z. Paal, R. Schloogl, J. Catal. 237 (2006) 17–28.
[28] O. Pozdnyakova, D. Teshner, A. Wootscha, J. Krohanert, B. Steinhauer, H. Sauer, L. Toth, F.C. Jentoft, A. Knop-Gericke, Z. Paal, R. Schloogl, J. Catal. 237 (2006) 1–16.
[29] T.A. Zepada, A. Martinez-hernandez, R. Guli-Lopez, B. Pawelec, Appl. Catal. B: Environ. 100 (2010) 450–462.
[30] P. Ratnaswami, D. Srinivas, C.V.V. Satyanarayana, P. Manikandan, R.S. Senthil Kumaran, M. Sachin, J. Catal. 221 (2004) 455–465.
[31] J.S. Margitfalvi, M. Hegedus, A. Szegedi, I. Sajo, Appl. Catal. A: Gen. 272 (2004) 87–97.
[32] F. Marino, C. Descormea, D. Dupreza, Appl. Catal. B: Environ. 58 (2005) 175–183.
[33] M. Kotobuki, A. Watanabe, H. Uchida, H. Yamashida, M. Watanabe, Appl. Catal. A: Gen. 236 (2005) 262–269.
[34] M. Kuriyama, H. Tanaka, S. Ito, T. Kubota, T. Miyao, S. Naito, K. Tomishige, K. Kunimori, J. Catal. 252 (2007) 39–48.
[35] A. Wootsch, C. Descorme, D. Duprez, J. Catal. 225 (2004) 259–266.
[36] F. Marino, C. Descorme, D. Duprez, Appl. Catal. B: Environ. 54 (2004) 59–66.
[37] M. Kotobuki, A. Watanabe, H. Uchida, H. Yamashita, M. Watanabe, Appl. Catal. A: Gen. 307 (2006) 275–283.
[38] G.W. Roberts, P. Chin, X. Sun, J.J. Spivey, Appl. Catal. B: Environ. 46 (2003) 601–611.
[39] M.P. Woods, P. Gawade, B. Tan, U.S. Ozkan, Appl. Catal. B: Environ. 97 (2010) 28–35.